J|A|C|S
ARTICLES
Published on Web 12/12/2007

Size-Dependent Charge Collection in Junctions Containing Single-Size and Multi-Size Arrays of Colloidal CdSe Quantum Dots

Emily A. Weiss,[‡] Ryan C. Chiechi,[‡] Scott M. Geyer,[§] Venda J. Porter,[§] David C. Bell,[†] Moungi G. Bawendi,*[,§] and George M. Whitesides*[,‡]

Department of Chemistry and Chemical Biology, Harvard University, 12 Oxford Street, Cambridge, Massachusetts 02138, Department of Chemistry, Massachusetts Institute of Technology, 77 Massachusetts Avenue, Cambridge, Massachusetts 02139,and Center for Nanoscale Systems, Harvard University, 11 Oxford Street, LISE 306, Cambridge, Massachusetts 02138

Received September 3, 2007; E-mail: gwhitesides@gmwgroup.harvard.edu; mgb@mit.edu

Abstract: This paper describes the electrical characteristics of junctions composed of three-dimensional arrays of colloidal CdSe quantum dots (QDs) with tin-doped indium oxide (ITO)/poly(3,4-ethylenedioxythiophene):poly(styrenesulfonate) (PEDOT:PSS) and eutectic Ga−In (EGaIn) electrodes. It focuses on a comparison of junctions containing QDs of one size to those of arrays containing QDs of multiple sizes. This comparison makes it possible to estimate the relative contributions of transport across various interfaces (e.g., between the QDs and between the QDs and the electrodes) to the observed electrical characteristics of the junction and to evaluate the dependence of these contributions on the locations of various sizes of QDs within the junction. The junctions were diodes, and their turn-on voltage depended on the size of the QDs next to the PEDOT:PSS. We describe this dependence using a Marcus model to estimate the barrier for charge transfer induced by the difference in energies between the orbitals of the QDs and the valence band of PEDOT:PSS.

Introduction

This paper examines the electrical characteristics of junctions composed of three-dimensional arrays of colloidal CdSe quantum dots (QDs). It focuses on a comparison of junctions containing QDs of one size to junctions containing QDs of multiple sizes (Figure 1). In all of these junctions, tin-doped indium oxide (ITO) covered with a thin layer of poly(3,4-ethylenedioxyl-thiophene):poly(styrene sulfonate) (PEDOT:PSS) supported the QDs, and a eutectic mixture of Ga and In (which we abbreviate as EGaIn)[1] served as a conformal top-contact. This comparison enabled us to infer some of the electronic consequences of quantum confinement that have been largely unexplored and unexploited in devices based on QDs. This work focuses on the importance of energetic alignment of the orbitals of the QDs and the work functions of the electrodes[2,3] in determining the shape of the current density−voltage ($J-V$) response and the turn-on voltage (V_{ON}) of the junctions. We observed that these junctions are diodes and that V_{ON} increases as the size of the QDs adjacent to the PEDOT:PSS decreases. We explained this trend using Marcus theory to estimate the barrier for charge transfer induced by the difference in energies between the orbitals of the QDs and the valence band of PEDOT:PSS. Understanding the dependence of the dark electrical characteristics of arrays of QDs on their size is critical if we are to exploit a major advantage of QDs as materials to be used in fabricating photonic devices such as solar cells, light-emitting diodes, and photodetectors: that is, the ability to tune their absorption and emission spectra by changing their size.[4,5]

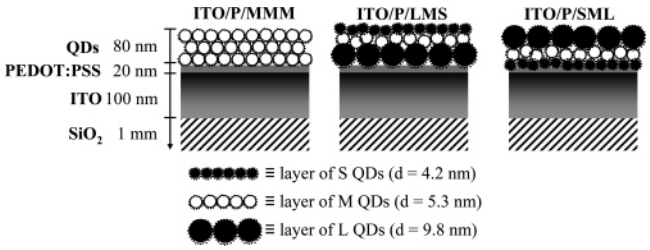

Figure 1. Schematic diagrams of selected films of QDs on ITO/PEDOT:PSS: ITO/P/MMM, ITO/P/LMS, and ITO/P/SML. The letters S, M, and L indicate small ($d = 4.2$ nm), medium ($d = 5.3$ nm), and large ($d = 9.8$ nm) CdSe QDs, respectively, and P indicates a ∼20-nm-thick layer of PEDOT:PSS. The nomenclature is explained in the text. Each row of QDs represents a layer that is 25−30 nm thick for the three-layer films or ∼38 nm thick for the two-layer films (not shown). The small dots around each QD represent the organic (butylamine) ligands. In the film, these ligands result in a nearest-neighbor distance of ∼0.2 nm between the QDs.

[‡] Department of Chemistry and Chemical Biology, Harvard University.
[§] Department of Chemistry, Massachusetts Institute of Technology.
[†] Center for Nanoscale Systems, Harvard University.

(1) Chiechi, R. C.; Weiss, E. A.; Dickey, M. D.; Whitesides, G. M. *Angew. Chem.*, Early View (doi:10.1002/anie.200703642), and references therein.
(2) Selmarten, D.; Jones, M.; Rumbles, G.; Yu, P.; Nedeljkovic, J.; Shaheen, S. *J. Phys. Chem. B* **2005**, *109*, 15927.
(3) Ginger, D. S.; Greenham, N. C. *Phys. Rev. B* **1999**, *59*, 10622.
(4) Murray, C. B.; Kagan, C. R.; Bawendi, M. G. *Annu. Rev. Mater. Sci.* **2000**, *30*, 545.

10.1021/ja076438h CCC: $40.75

Nomenclature. We use the letters S, M, and L to designate small ($d = 4.2$ nm), medium ($d = 5.3$ nm), and large ($d = 9.8$ nm) CdSe quantum dots, respectively, and P to indicate a ~20-nm-thick layer of PEDOT:PSS (Figure 1). For example, the film ITO/P/SML comprised stacked layers (where each layer was a multilayer, not a monolayer) of each of the S, M, and L QDs spun, successively, onto the glass/ITO/PEDOT:PSS substrate, where the layer of S QDs was adjacent to the PEDOT:PSS. The junction ITO/P/SML/EGaIn was an ITO/P/SML film with the layer of large QDs contacting the EGaIn electrode. The shorthand "junction SML" means the junction ITO/P/SML/EGaIn, and ITO/P/L**X**/EGaIn is a junction with L QDs adjacent to the PEDOT:PSS layer and an unspecified combination of QDs (**X**) in the rest of the array. The notation $|V_{ON}|$(SL) means the absolute value of the turn-on voltage for the junction ITO/P/SL/EGaIn. The symbol V is the bias applied to the junction—that is, the difference in voltage between the ITO and the EGaIn electrodes. When V is positive, EGaIn is biased positively with respect to ITO (i.e., electrons flow from ITO to EGaIn).

Background: Quantum Confinement. Semiconductor QDs are clusters of atoms with dimensions on the order of the size of the exciton in the bulk material (these dimensions are derived from the exciton binding energy measured from optical absorption, luminescence, or photoionization experiments).[6−9] The boundary of the QD confines charge carriers and excitons in all three spatial dimensions; this confinement collapses the continuous density of states of the bulk semiconductor into discrete electronic states and concentrates the bulk oscillator strength into discrete transitions. One consequence of quantum confinement is that the distribution of states of a QD begins to resemble that of a molecule:[4,5,8,10,11] smaller dots have increased separation between energy levels, higher energy band-edge absorptions,[4,8,12,13] and more negative reduction potentials.[14]

Experimental Design

Materials. Arrays of CdSe QDs are popular model systems for studying optical and electronic quantum size effects. Many groups[15−22] now routinely synthesize macroscopic quantities of monodisperse (σ < 4% rms) CdSe QDs at temperatures less than 400 °C using wet-chemical procedures. The QDs have diameters ranging from 1.2 to 15 nm (the bulk exciton radius of CdSe is ~5 nm[9]), good electronic passivation, and uniform shape.[15,23,24] These synthetic methods make CdSe QDs useful and highly developed building blocks for the fabrication of superlattices ordered over hundreds of micrometers,[4,25−27] with controllable nearest-neighbor distances.[4,10] Furthermore, CdSe QDs have a finely tuned profile of absorption vs size with good coverage of the visible spectrum: for $d = 1.2-15$ nm, the band gap (E_g) ranges from 2.9 eV (~425 nm) to 1.75 eV (~710 nm).[4,10,13,15,28−30]

Studies of junctions incorporating ITO electrodes are relevant to the development of a wide range of devices: ITO is the most commonly used transparent conducting oxide for organic and dye-sensitized photovoltaics, light-emitting diodes, electrochromics, electroluminescent devices, displays, and heat-reflective coatings.[31] Often, ITO is coupled with the polymeric hole-conductor PEDOT:PSS, which is, conveniently, spin-coated from commercially available aqueous suspensions. This polymer is effectively transparent throughout the long-wavelength UV and visible regions of the spectrum and provides a conformal contact between the active material (here, QDs) and the rough, hydrophilic surface of ITO for faster collection of charge.[32]

The use of EGaIn as a top-contact makes it practical to fabricate junctions incorporating QDs easily and in high yield.[1] The eutectic point of Ga−In alloy occurs at ~25% indium, at which composition the melting point is 15.7 °C. Eutectic Ga−In is used commercially as a high-performance, electrically conductive lubricant but has not yet been widely exploited as an electrode in thin-film devices. Its non-Newtonian behavior make it very well suited for this use: it flows like a liquid but holds its shape once the stress it experiences on its surface falls below a characteristic threshold value (~1 N/m). EGaIn can therefore form conformal contacts that are smaller than those formed with Hg (the other metal popular for liquid electrodes[33]) when extruded through apertures of the same diameter.[1] Unlike the evaporation of a top-contact of a solid metal with a high melting point (typically gold), the fabrication of solid−EGaIn junctions does not damage reactive organic materials or form persistent metal filaments that short the junction or cause artificially high currents.[34,35] Eutectic Ga−In junctions are, in general, more stable and have lower associated toxicity than Hg-drop junctions, and they have the potential for use in practical devices.[1] Eutectic Ga−In is particularly suited as an electrode for use with CdSe QDs because its work function (WF, which we assume to be some value between that of In, WF(In) = 4.1 eV, and that of Ga, WF(Ga) = 4.2 eV)[36] is close to the energies of their LUMOs; EGaIn can, therefore, easily exchange electrons with the QDs, unlike Au (WF = 5.3 eV). Using the conformal EGaIn electrode, we were able to produce five or more junctions per 1-cm^2 sample (over 14 samples, two per type of array) of junctions; approximately 95% of the junctions we formed

(5) Grundmann, M.; Christen, J.; Ledentsov, N. N.; Bohrer, J.; Bimberg, D. *Phys. Rev. Lett.* **1995**, *74*, 4043.
(6) Pan, D.; Towe, E. *Appl. Phys. Lett.* **2000**, *76*, 3301.
(7) Wise, F. W. *Acc. Chem. Res.* **2000**, *33*, 773.
(8) Ekimov, A. I.; Hache, F.; Schanne-Klein, M. C.; Ricard, D.; Flytzanis, C.; Kudryavtsev, I. A.; Yazeva, T. V.; Rodina, A. V. *J. Opt. Soc. Am. B* **1993**, *10*, 100.
(9) Kittel, C. *Introduction to Solid State Physics*, 7th ed.; John Wiley and Sons: New York, 1996.
(10) Kagan, C. R.; Murray, C. B.; Bawendi, M. G. *Phys. Rev. B* **1996**, *54*, 8633.
(11) Banin, U.; Cerullo, G.; Guzelian, A. A.; Bardeen, C. J.; Alivisatos, A. P. *Phys. Rev. B* **1997**, *55*, 7059.
(12) Klimov, V. I.; Mikhailovsky, A. A.; Xu, S.; Malko, A.; Hollingsworth, J. A.; Leatherdale, C. A.; Eisler, H.-J.; Bawendi, M. G. *Science* **2000**, *290*, 314.
(13) Norris, D. J.; Bawendi, M. G.; Brus, L. E. Optical Properties of Semiconductor Nanocrystals. In *Molecular Electronics*; Jortner, J., Ratner, M. A., Eds.; Blackwell Science Ltd.: Malden, MA, 1997; p 281.
(14) Tarucha, S.; Austing, D. G.; Honda, T.; van der Hage, R. J.; Kouwenhoven, L. P. *Phys. Rev. Lett.* **1996**, *77*, 3613.
(15) Murray, C. B.; Norris, D. J.; Bawendi, M. G. *J. Am. Chem. Soc.* **1993**, *115*, 8706.
(16) Snee, P. T.; Chan, Y.; Nocera, D. G.; Bawendi, M. G. *Adv. Mater.* **2005**, *17*, 1131.
(17) Boatman, E.; Lisensky, G. C.; Nordell, K. J. *J. Chem. Educ.* **2005**, *82*, 1697.
(18) Li, J. J.; Wang, Y. A.; Guo, W.; Keay, J. C.; Mishima, T. D.; Johnson, M. B.; Peng, X. *J. Am. Chem. Soc.* **2003**, *125*, 12567.
(19) Peng, X.; Wickham, J.; Alivisatos, A. P. *J. Am. Chem. Soc.* **1998**, *120*, 5343.
(20) Shim, M.; Wang, C.; Guyot-Sionnest, P. *J. Phys. Chem.* **2001**, *105*, 2369.
(21) Talapin, D. V.; Shevchenko, E. V.; Kornowski, A.; Gaponik, N.; Haase, M.; Rogach, A. L.; Weller, H. *Adv. Mater.* **2001**, *13*, 1868.
(22) Munro, A. M.; Plante, I. J.-L.; Ng, M. S.; Ginger, D. S. *J. Phys. Chem. C* **2007**, *111*, 6220.
(23) Bowen Katari, J. E.; Colvin, V. L.; Alivisatos, A. P. *J. Phys. Chem.* **1994**, *98*, 4109.
(24) Peng, Z. A.; Peng, X. *J. Am. Chem. Soc.* **2001**, *123*, 183.
(25) Sun, B.; Marx, E.; Greenham, N. C. *Nano Lett.* **2003**, *3*, 961.
(26) Huynh, W. U.; Dittmer, J. J.; Teclemariam, N.; Milliron, D. J.; Alivisatos, A. P. *Phys. Rev. B* **2003**, *67*, 115326.
(27) Yu, G.; Gao, J.; Hummelen, J. C.; Wudi, F.; Heeger, A. J. *Science* **1995**, *270*, 1789.
(28) Kagan, C. R. Basic Physics of Semiconductor Quantum Dots; Proceedings of the NSF−Conicet Quilmes Nanoscience Workshop, 2003, Quilmes, Provincia de Tucuman, Argentina.
(29) Greenham, N. C.; Peng, X.; Alivisatos, A. P. *Phys. Rev. B* **1996**, *54*, 17628.
(30) Landsberg, P. T.; Nussbaumer, H.; Willeke, G. *J. Appl. Phys.* **1993**, *74*, 1451.
(31) Cui, J.; Wang, A.; Edleman, N. L.; Ni, J.; Lee, P.; Armstrong, N. R.; Marks, T. J. *Adv. Mater.* **2001**, *13*, 1476.
(32) Ouyang, J.; Chu, C.-W.; Chen, F.-C.; Xu, Q.; Yang, Y. *Adv. Funct. Mater.* **2005**, *15*, 203.
(33) Weiss, E. A.; Chiechi, R. C.; Kaufman, G. K.; Kriebel, J. K.; Li, Z.; Duati, M.; Rampi, M.-A.; Whitesides, G. M. *J. Am. Chem. Soc.* **2007**, *129*, 4336.
(34) Beebe, J. M.; Kushmerick, J. G. *Appl. Phys. Lett.* **2007**, *90*, 083117.
(35) Ssenyange, S.; Yan, H.; McCreery, R. L. *Langmuir* **2006**, *22*, 10689.
(36) Sze, S. M. *Physics of Semiconductor Devices*, 2nd ed.; John Wiley and Sons: New York, 1981.

were functional—that is, they did not short from contact between the ITO or the PEDOT:PSS and the EGaIn through defects in the film of QDs.

Arrays of QDs of Multiple Sizes. Incorporation of an array of QDs having multiple sizes into an electrical junction has the potential to allow (i) independent variation of the separation in energy levels between the QDs and each of the electrodes and (ii) the presence of a gradient in potential (a set of steps in the energy of the LUMOs) within the array of QDs, along which electrons can, in principle, cascade from the smallest to the largest QDs. This cascade suggests strategies for achieving efficient vectorial transport of electrons to an electrode. Comparing the electrical characteristics of the arrays of multiple sizes of QDs with those of the arrays of only a single size helped us to separate the contribution of charge transfer at the interface between the QDs and PEDOT:PSS from that of charge transfer within the array to the overall $J-V$ response. In a complementary publication[37] on the photonic properties of junctions of the same fabrication and structure as those in this study, we utilize the arrays of multiple sizes of QDs to perform spatially selective photoexcitation of the QDs, in order to clarify the mechanism for generation and flow of photocurrent in the junctions.

Prior Work. Many groups have studied the dark conductivity of three-dimensional colloidal glasses and crystals of CdSe QDs.[38−41] The mobility of electrons and holes in an array of CdSe QDs depends, in part, on the size of the QDs in the array: (i) the number of interfaces between QDs—interfaces that are resistive elements[42,43]—increases for an array of a given thickness as the size of the QDs in the array decreases, and (ii) the density of trap sites (Cd^{2+} and Se^{2-} ions on the surface of the QDs to which organic ligands are not bound) increases as the size of the QDs in the array decreases because smaller QDs have a higher ratio of surface area to volume.[44,45]

Several groups have accomplished directional control of charge transfer—one possible application for the ordered arrays incorporating multiple sizes of QDs—in systems that have components with multiple oxidation and reduction potentials: arrays of porphyrins,[46] within dendrimers,[47] and in a columnar array of vertically coupled InAs/GaAs QDs.[48]

Much work[26,29,43,49] has focused on electron transport at the interface between QDs and polymer in the context of photoinduced charge separation in solar cells, where the QDs (the *n*-type material) transport electrons and the polymer (the *p*-type material) transports holes. In the case of a "zero-bias device" like a solar cell, the ionization of excitons (separation of excitons into electron−hole pairs) occurs spontaneously only at the heterojunction, while an applied electric field would be needed to split excitons within the portion of the film of QDs or polymer away from the interface. In this work, we inject electrons and holes from electrodes rather than creating them from photoexcitation, but we discuss many of the same factors that govern the transport of charge across the heterogeneous interface between QDs and a polymer in a solar cell: alignment of donor and acceptor energy levels, overlap of orbitals, and the presence of electric fields.

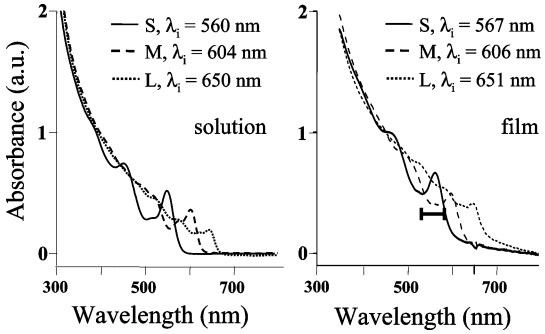

Figure 2. Ground-state absorption spectra of the S, M, and L QDs in a solution in hexanes (left, with concentrations 1×10^{-5} M (L), 6.5×10^{-5} M (M), and 1×10^{-4} M (S)) and in butylamine-treated films (right) spun on glass from $CHCl_3$ solutions of the same concentrations. The symbol λ_i indicates the wavelength of the maximum of the band-edge absorption (the $1S_{3/2} \rightarrow 1S_e$ transition). This maximum is at lower energy in the spectra of the films than in the spectra of the solutions due to electronic interaction between the QDs in the film. The full width at half-maximum of the band-edge peak of the S QDs is indicated in the spectra of the films; this width (of the peak for each size of QD) equals the uncertainty in the energy of the LUMO for that QD.

Results and Discussion

Preparation and Microscopic Characterization of Films of QDs on ITO/PEDOT:PSS. The Supporting Information describes the (published[16]) solution-phase synthesis of colloidal CdSe QDs. We prepared three sizes of nanocrystals, with band-edge absorption maxima at $\lambda_i = 560$ nm (S), 604 nm (M), and 650 nm (L) (measured as ground-state absorption in a solution in hexanes; Figure 2, left). We used trioctylphosphine oxide (TOPO) as the organic capping layer for all of the QDs *in solution*. Following previous methods for making close-packed QD films,[15,28,50−53] we suspended the QDs in methanol and precipitated the QDs from this suspension three times.

The films of QDs were vertical stacks of layers of CdSe QDs, with each layer having QDs of the same diameter (Figure 1). We produced seven different types of films, each composed of either two or three layers of dots: ITO/P/**X**, with **X** = LLL, MMM, SSS, SML, LMS, SL, and LLS. We began the preparation of each film by spin-coating PEDOT:PSS (Baytron-P) from a 2:1 dilution of the commercially available aqueous suspension (Bayer, conductive grade) in deionized water at 5000 rpm for 1 min onto ITO (on float glass, Delta Technologies, $R = 8-12\ \Omega$/square) that had been cleaned with ethanol and dried in a stream of N_2. The PEDOT:PSS film was annealed in a vacuum oven at ∼1 mTorr and 100 °C for 30 min.

We then spin-coated the QDs, one layer at a time, at 5000 rpm for 1 min from solutions in $CHCl_3$ in the following concentrations (estimated from the absorption of the solution at 350 nm[54]): 1×10^{-5} M (L), 6.5×10^{-5} M (M), 1×10^{-4} M (S) for the three-layer films and 1.5×10^{-5}M (L) and 1.6×10^{-4} M (S) for the two-layer film. This combination of

(37) Weiss, E. A.; Porter, V. J.; Chiechi, R. C.; Geyer, S. M.; Bell, D. C.; Bawendi, M. G.; Whitesides, G. M. *J. Am Chem. Soc.* **2007**, ASAP (ja076439+).
(38) Drndic, M.; Jarosz, M. V.; Morgan, N. Y.; Kastner, M. A.; Bawendi, M. G. *J. Appl. Phys.* **2002**, *92*, 7498.
(39) Morgan, N. Y.; Leatherdale, C. A.; Drndic, M.; Jarosz, M. V.; Kastner, M. A.; Bawendi, M. G. *Phys. Rev. B* **2002**, *66*, 075339.
(40) Yu, D.; Wehrenberg, B. L.; Jha, P.; Ma, J.; Guyot-Sionnest, P. *J. Appl. Phys.* **2006**, *99*, 104315.
(41) Yu, D.; Wang, C. J.; Wehrenberg, B. L.; Guyot-Sionnest, P. *Phys. Rev. Lett.* **2004**, *92*, 216802.
(42) Brust, M.; Bethell, D.; Schiffrin, D. J.; Kiely, C. J. *Adv. Mater.* **1995**, *7*, 795.
(43) Ginger, D. S.; Greenham, N. C. *J. Appl. Phys.* **2000**, *87*, 1361.
(44) Ejit, S. W. H.; van Veen, A.; Schut, H.; Mijnarends, P. E.; Denison, A. B.; Barbellini, B.; Bansil, A. *Nat. Mater.* **2006**, *5*, 23.
(45) Biju, V.; Makita, Y.; Nagase, T.; Yamaoka, Y.; Yokoyama, H.; Baba, Y.; Ishikawa, M. *J. Phys. Chem. B* **2005**, *109*, 14350.
(46) Coon, D. D.; Karunasiri, R. P. G. *Appl. Phys. Lett.* **1984**, *45*, 649.
(47) Johnson, H. T.; Bose, R.; Robinson, H. D.; Goldberg, B. B. *Appl. Phys. Lett.* **2003**, *82*, 3382.
(48) Caroli, C.; Combescot, R.; Nozieres, P.; Saint-James, D. *J. Phys. C* **1971**, *4*, 916.
(49) Huynh, W. U.; Dittmer, J. J.; Alivisatos, A. P. *Science* **2002**, *295*, 2425.
(50) Porter, V. J.; Mentzel, T.; Charpentier, S.; Kastner, M. A.; Bawendi, M. G. *Phys. Rev. B* **2006**, *73*, 155303/1.
(51) Murray, C. B.; Kagan, C. R.; Bawendi, M. G. *Science* **1995**, *270*, 1335.
(52) Leatherdale, C. A.; Kagan, C. R.; Morgan, N. Y.; Empedocles, S. A.; Kastner, M. A.; Bawendi, M. G. *Phys. Rev. B* **2000**, *62*, 2669.
(53) Jarosz, M. V.; Porter, V. J.; Fisher, B. R.; Kastner, M. A.; Bawendi, M. G. *Phys. Rev. B* **2004**, *70*, 195327/1.
(54) Leatherdale, C. A.; Woo, W.-K.; Mikulec, F. V.; Bawendi, M. G. *J. Phys. Chem. B* **2002**, *106*, 7619.

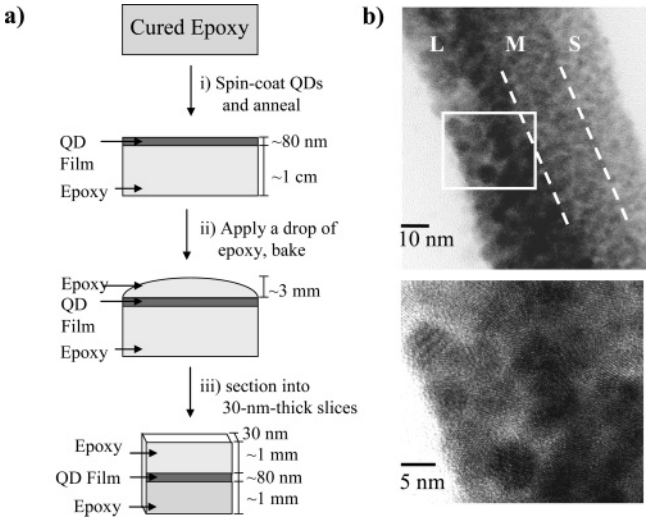

Figure 3. (a) Schematic diagram of the process used to make the TEM samples: (i) We spun a film of QDs (using the same conditions as given in the text for the three-layer films on ITO/P) onto a slab of thermally cured epoxy (annealed at 60 °C for 6 h). (ii) A drop of the pre-polymer of the same epoxy was applied to the top of the QD film, and the sample was heated at 70 °C for 12 h. We then trimmed the block with a razor blade to expose to the blade a square surface with an area of approximately 1 mm^2 and mounted the block in the ultramicrotomy chuck. (iii) A microtome sliced 30-nm-thick cross sections of the epoxy−QD composite. (b) Top: TEM micrograph of a cross section of the SML QD film spun onto, and subsequently embedded in, epoxy (on a lacey carbon grid). The white dashed lines indicate the boundaries between layers of QDs of different size. Bottom: High-resolution TEM image (of the boxed region in the top image) showing the crystal lattice of individual QDs.

concentrations and spinning conditions yielded layers that were ~26−29 nm thick each for the three-layer films (as measured by AFM, Figure S1). For each layer of the two-layer films, we used a concentration of solution of QDs that—according to a previously constructed calibration curve of the absorbance at 350 nm vs the thickness of the film (measured by AFM)[55]—corresponded to ~38 nm thick film.

After the deposition of each layer, we soaked the film in a 0.1 M solution of butylamine in acetonitrile to exchange the TOPO ligands for butylamine ligands[53] and annealed it at 70 °C for 1 h to drive off any excess (unbonded) organic material and to reorganize the butylamine ligands into a more closely packed, presumably intercalated configuration.[53] Treatment of films of CdSe QDs with butylamine, and subsequent annealing at this temperature, has been shown to result in ~0.2 nm separation between the dots, as determined by glancing angle X-ray scattering.[53] Figure 2 (right) shows ground-state absorbance spectra of the butylamine-treated films, in which λ_i is slightly higher than its value in solution for each of the sizes of QDs. The bathochromic shift of the peaks in the absorption spectra reflects an increase in the degree of delocalization of the excitonic wavefunction on going from solution to solid-state array.

Figure 3a shows the procedure we used to prepare a cross section of the multi-size film for imaging by transmission electron microscopy (TEM). We spun three layers of QDs (S, then M, then L) onto a 5-mm-thick slab of epoxy (Araldite 502) that had been cured in an oven at 60 °C for 6 h. We then applied a drop (~0.25 mL) of the pre-polymer of the same epoxy to the top of the film to embed the entire sample, baked the sample for at 70 °C for 12 h, and, using an ultramicrotome (Leica), cut ~30-nm-thick slices of the embedded film. Figure 3b shows TEM images of such a sample on a lacey carbon grid at two different magnifications. Both images clearly show three distinct layers of QDs of different sizes. The layer of small dots is thinner than 25 nm, probably because the spinning conditions were not optimized for the epoxy substrate. The bottom image shows the lattice fringes of the individual QDs. We also note that the L QDs appear to be ~7.5 nm in diameter rather than the 9.8 nm obtained from solution-phase absorption measurements. There are several sources of error in estimating the diameter of the QDs from this particular TEM image that would possibly combine to account for this discrepancy: (i) The QDs that we imaged most clearly were those at the edge of the sample (where the cross-section was thinnest), but any portion of those QDs that was embedded in the epoxy medium (which includes the QDs near the edge of the sample) are effectively invisible using this technique, so the QDs appear smaller than they actually are. (ii) There is some distortion of the image due to the fact that we probed a multilayer cross section, not a monolayer (as is usually used to estimate the size of QDs). (iii) There is a 1−3% error expected in the size of the scale bar.

Formation of the ITO/P/QD/EGaIn Junctions and *J*−*V* Measurements. Figure S2 shows the procedure we used to prepare EGaIn tips at ambient temperature (~298 K) and under ambient atmosphere. We (i) drew EGaIn into a 10-μL gastight glass syringe with a permanently affixed metal needle that had been squared off and dulled using a metal file and 1500-grit sandpaper, (ii) extruded a small (~0.1 μL) drop of EGaIn (Aldrich, 99.99+%, mp ≈ 15.7 °C, used as-received), (iii) brought the drop in contact with the bare Ag surface of an evaporated film, to which it adhered, and (iv) slowly (~50 μm/s) raised it until the EGaIn separated completely into a drop left on the surface and a drop on the needle. The drop of EGaIn (~0.05 μL) on the needle, which had a tapered shape, was used to form the top-contact for the junction. The EGaIn remaining on the surface of the Ag was discarded. We brought this tapered drop into contact with the QD film, imaged the junction with a digital camera at 315× magnification, and measured the diameter of the interface between the QDs and EGaIn on a size-calibrated computer screen (Figure 4). Connecting a portion of the surface of the sample where the ITO was exposed to a common electrode (ground) via a gold needle completed the circuit. Electrons flowed from ITO to EGaIn when the EGaIn was biased positively with respect to the ITO ($V > 0$), and from EGaIn to ITO when the EGaIn was biased negatively with respect to the ITO ($V < 0$).[56]

We collected current−voltage (I−V) data by scanning V in a range from $V = -2.0$ to $+2.0$ V (in steps of 0.2 V), and in a range from $V = -0.5$ to $+0.5$ V (in steps of 0.05 V) for the junctions LLL, LMS, LLS, and MMM, which required more data at these low values of V in order to determine the turn-on voltage (V_{ON}). We recorded the current after allowing the junction to equilibrate at the specified V for 2 s and divided the current by the area of the junction to obtain the current density (J). For the range $V = -x$ to $+x$, one J−V trace was defined as

(55) Porter, V. J. Exploring and Enhancing Conductivity in Semiconductor Nanoparticle Films. Ph.D. dissertation, Massachusetts Institute of Technology, 2007.

(56) The direction of flow of electrons is formally opposite that of current, so, at $V > 0$, the current flows from EGaIn through the QDs to ITO, and at $V < 0$, the current flows from ITO through the QDs to EGaIn.

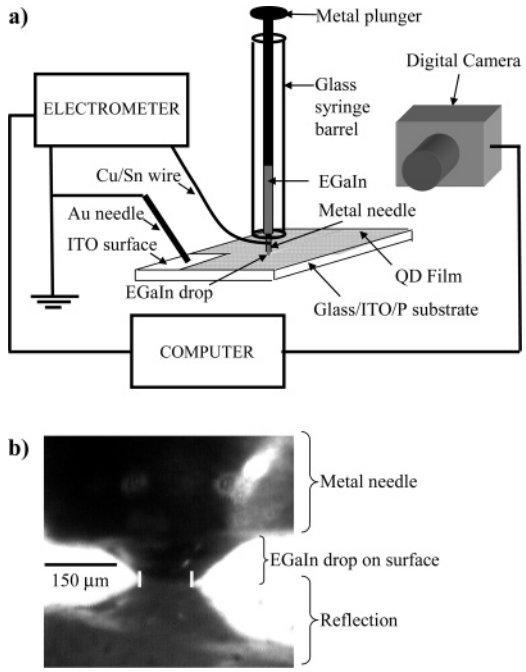

Figure 4. (a) Schematic illustration of an ITO/P/QD/EGaIn junction. The electrical circuit was as follows: The EGaIn connected electrically to the metallic needle of the syringe. The electrometer connected to the metallic needle via a metal wire (made of solid-core Cu/Sn alloy, a common corrosion-resistant conductor) wrapped around the needle. A micromanipulator brought the EGaIn into contact with the QD film (at $T = 298$ K) and the ITO electrode connected to ground via a gold needle (tungsten or platinum could substitute for gold) in mechanical contact with an exposed area of the ITO surface. We imaged the junction from the side with a digital camera. (b) Digitized, magnified image of the EGaIn drop in contact with a film of QDs. The drop reflects from the surface of the metal stage on which the QD film (on a transparent glass/ITO substrate) sits. We estimated the diameter of the junction for the calculation of J (A/cm^2) by measuring the width of the interface between drop and its reflection (the distance between the two white, vertical lines in this photograph). The diameters (areas) of the junctions ranged from ~80 to ~150 μm (5.0×10^{-5}–5.0×10^{-4} cm^2).

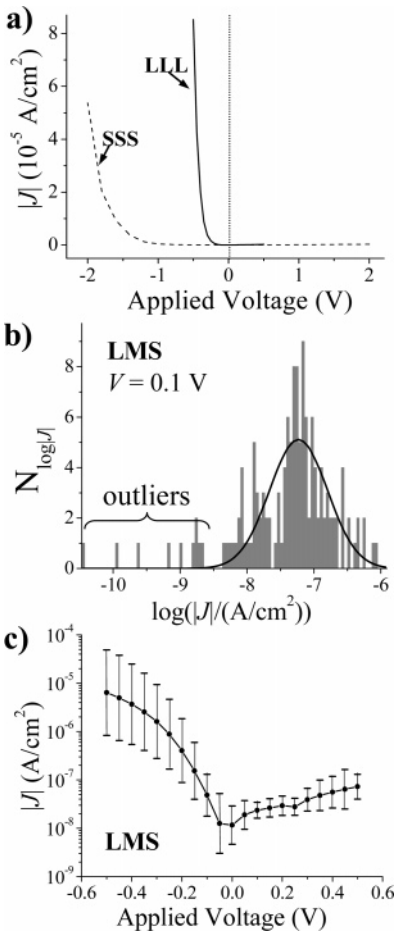

Figure 5. (a) Plots of the absolute value of $\langle J\rangle_{\log}$ vs V for the junctions ITO/P/**X**/EGaIn, **X** = LLL ($V = +0.5$ V → -0.5 V) and **X** = SSS ($V = +2.0$ V → -2.0 V). The junctions are diodes: electrons flow from EGaIn to ITO, but not vice versa. Table 1 lists the turn-on voltages, V_{ON}, for each junction. (b) A histogram of all measured values of log $|J|$ (with 100 bins) for **X** = LMS at $V = 0.1$ V. The y-axis, $N_{\log|J|}$, is the number of times we recorded the each value of log$|J|$. We fit the histogram with a Gaussian function with standard deviation σ (= 0.43) (see Figure S3 for additional histograms). (c) Plot of the absolute value of $\langle J\rangle_{\log} \pm \sigma$ vs voltage for the junction **X** = LMS. Data from at least four locations on each of two separately prepared samples—for a total of 138 values of J—were used to compute the average and the uncertainty. Figure S4 contains the plots for the junctions LLL, LLS, MMM, SL, SML, and SSS.

$0 \rightarrow +x \rightarrow -x \rightarrow 0$. Figure 5a shows plots of J vs V for the junctions LLL and SSS. These plots are intended to illustrate the shape of the J–V curves; Figure 5b,c shows the error analysis. The asymmetry of the J–V curves around $V = 0$ V is representative of that for all of the junctions. They are diodes: electrons flow—at values of V more negative than V_{ON}—from EGaIn to ITO, but not appreciably from ITO to EGaIn.[57]

The value for J for a particular V in Figure 5a is the log-mean of J ($\langle J\rangle_{\log} = 10^{\langle \log J\rangle}$, where $\langle \log J\rangle$ is the mean value of log($|J|$)). We used $\langle J\rangle_{\log}$ because we observed that, with the exception of **X** = SL, the values for log($|J|$) appeared to be distributed approximately normally, while the values for J did not.[33] Figure 5b gives an example of a histogram for the values of log($|J|$) for the junction LMS, and Figure S3 contains additional histograms for the values of J and log($|J|$). One explanation for the apparent normal distribution of log($|J|$) is that J depends exponentially on a physical parameter that is distributed normally, such as the electric field (E) across the junction ($E = V/L$, where L is the thickness of the junction). In that case, inhomogeneous disorder in L could cause L (and, in turn, E) to be distributed normally and would lead to the observed variation in J. There did exist "outliers"—points that were two to three standard deviations either above or below the mean value of log($|J|$) (Figures 5b and S3)—in many of the histograms, but we did not observe a trend in the values of log($|J|$) for these outliers. We presume that they were due to measurement of current through a defect in the film, such as a pinhole, or to contact resistance due to adsorbates on the film.

Figure 5c shows a plot of the absolute value of $\langle J\rangle_{\log}$ vs V for the junction LMS (see Figure S4 for the plots for the rest of the junctions). The standard deviation (σ) of the Gaussian functions used to fit each of the histograms (using the nonlinear least-squares fitting algorithm in OriginPro 7) yielded the error bars in this figure—that is, each point is $\langle J\rangle_{\log} \pm \sigma$. We used data from at least four locations on each of two separately prepared samples (for a total of 138 values of J for LMS) to compute $\langle J\rangle_{\log}$ and σ. For **X** = SL, neither J nor log($|J|$) appeared to be distributed normally, possibly because SL was the junction

(57) Occasionally, when a value of V between +1.0 and +2.0 V was applied, the QD junctions failed: the current density increased suddenly by one or more orders of magnitude. Failure of the devices was probably caused by a build-up of negative charge in the PEDOT:PSS layer; accumulation of negative charge leads to over-reduction and ultimately dielectric breakdown.

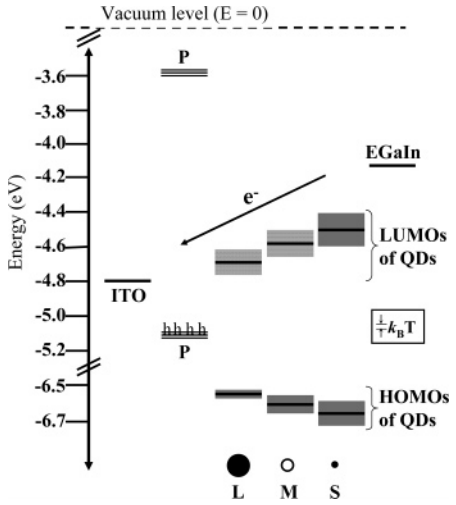

Figure 6. Energy diagram for the components of the ITO/P/QD/EGaIn junctions: the Fermi level of ITO (before thermal equilibration with EGaIn), the valence and conduction bands of PEDOT:PSS, the HOMOs and LUMOs of the S, M, and L dots (calculated as explained in the text), and the Fermi level of EGaIn (before thermal equilibration with ITO). The gray boxes indicate the uncertainty in the energies of the HOMOs and LUMOs of the QDs (also explained in the text). The arrow indicates the direction that the electrons move when $V > 0$, where the device turns on. The symbol "h" in the VB of PEDOT:PSS indicates the presence of uncharged (counterion-stabilized) holes.

on which we gathered the fewest values (30). For $\mathbf{X} = \mathrm{SL}$, the average values of J plotted in Figure S4 are $\langle J \rangle_{\log}$, but the error bars equal the total range in J that we measured, rather than σ.

Electronic Structure of the Junctions. Figure 6 shows a simplified electronic structure diagram of the (unconnected) components of the ITO/P/QD/EGaIn junction; we will use this diagram to discuss the observed electrical characteristics of the junction. The diagram summarizes the energy levels of the highest occupied molecular orbital (HOMO) and lowest unoccupied molecular orbital (LUMO) for each size of QD, the work functions of ITO[58] and EGaIn,[36,59] and the conduction band (CB) and valence band (VB) of PEDOT:PSS.

It has not been determined definitively whether the HOMO and LUMO of a CdSe QD split symmetrically or asymmetrically from the energies of the VB and CB, respectively, of bulk CdSe, as the size of the QD decreases and its optical band gap (E_g) increases. The argument for an asymmetric splitting is that, in CdSe, the effective mass of the electron is significantly smaller than the effective mass of the hole ($m_e = 0.13m_o$, $m_h = 1.14m_o$, where m_o is the mass of a free electron);[60] according to the effective mass approximation (EMA),[60] most of the increase in E_g (specifically, ~75% of the increase) from larger QDs to smaller QDs therefore should appear as a shift in their LUMOs. The results of more sophisticated theoretical methods[61,62] have suggested a symmetric splitting of energy levels (or at least more symmetric than that given by the EMA); a symmetric splitting gives $E_{\mathrm{HOMO}}(\mathrm{QD}) = E_{\mathrm{VB}}(\text{bulk CdSe}) - (E_g(\mathrm{QD}) - E_g(\text{bulk CdSe}))/2$, and $E_{\mathrm{LUMO}}(\mathrm{QD}) = E_{\mathrm{CB}}(\text{bulk CdSe}) + (E_g(\mathrm{QD}) - E_g(\text{bulk CdSe}))/2$. The difference between the results obtained from the symmetric splitting and those obtained from the asymmetric splitting is minimal (0.1 eV or less), and the set of conclusions that we draw in this work would hold true no matter which we chose; nonetheless, for the sake of completeness, the energies of the HOMOs and LUMOs of the QDs in Figure 3 are an average of the energies obtained from these two methods. The energy calculated assuming an asymmetric splitting dictates the upper bound of the uncertainty in the energy of the HOMO (top of the gray box); the energy calculated assuming a symmetric splitting dictates the lower bound of the uncertainty in the energy of the HOMO (bottom of the gray box). The uncertainty in the energies of the LUMOs of the QDs is the full width at half-maximum of the band-edge absorption peaks that yielded E_g; this width is larger than the difference between the energies calculated from the two methods.

Origin of Rectification. (1) The "Off" State. In all of the junctions, only a small ($\sim 10^{-8}$–10^{-7} A/cm^2) leakage current results from the net flow of electrons from the ITO to the EGaIn—that is, transport of electrons from ITO to EGaIn, transport of holes from EGaIn to ITO, or some combination of the two. There are two aspects of these devices that strictly limit the rates of both of these processes (at least at the values of V we applied: 0 V → +2.0 V), as shown in Figure 6: (i) EGaIn cannot inject holes into the QDs (that is, oxidize the QDs) because the values of V that we applied were not large enough to bring the energies of the HOMOs of the QDs (~ −6.5 to −6.7 eV) above the Fermi level of EGaIn (~ −4.15 eV). (ii) Electrons that arrived at the interface between PEDOT:PSS and the QDs were trapped (because the VB of PEDOT:PSS (~ −5.2 eV) is lower in energy than the LUMOs of the QDs (~−4.8 to −4.6 eV), and because there were no holes in the QD layer with which to combine). We suspect that the leakage current we did observe resulted from electrons that were thermally excited from the VB to the CB of the PEDOT:PSS, which has a smaller band gap (~1.5 eV) than do the QDs (~2 eV), and then injected into the LUMOs of the adjacent QDs.

The junction ITO/P/EGaIn (with no QDs) showed the same diode-like behavior as the junctions with the QDs (Figure S5). The trapping of electrons injected from ITO in the film of PEDOT:PSS manifested itself as hysteresis in the J–V curve for the ITO/P/EGaIn junction.

(2) The "On" State. We did observe the flow of electrons from EGaIn to ITO when EGaIn was biased negatively with respect to the ITO (for $|V| > |V_{\mathrm{ON}}|$) through, we believe, three processes: (i) EGaIn injected electrons into the LUMOs of the layers of QDs until the energy required for further injection exceeded V. At this "saturation" point, some fraction of the QDs were reduced (that is, they contained an extra electron; we denote them " QD^- ").[52,63] (ii) To maintain overall neutrality of charge at the interface between the QDs and the PEDOT:PSS, positive charges injected from the ITO collected in the PEDOT:PSS and moved to this interface. (iii) Charge annihilation—combination of electrons from the QDs and holes from the PEDOT:PSS due to electron transfer from the LUMO of the QDs to the HOMO of PEDOT:PSS (a process that dissipates

(58) Ishii, H.; Sugiyama, K.; Ito, E.; Seki, K. *Adv. Mater.* **1999**, *11*, 605.
(59) In Figure 6, the Fermi energies of the electrodes (EGaIn and ITO) are drawn at their levels before thermal equilibration of the population of the electrons in the electrodes occurs. This equilibration results in a more negative (by ~0.35 eV) Fermi level for EGaIn and a less negative (by ~0.35 eV) Fermi level for ITO.
(60) Norris, D. J.; Bawendi, M. G. *Phys. Rev. B* **1996**, *53*, 16338.
(61) Franceschetti, A.; Zunger, A. *Phys. Rev. Lett.* **1997**, *78*, 915.
(62) He, L.; Bester, G.; Zunger, A. *Phys. Rev. Lett.* **2005**, *95*, 246804.
(63) Alperson, B.; Cohen, S.; Rubinstein, I.; Hodes, G. *Phys. Rev. B* **1995**, *52*, R17017.

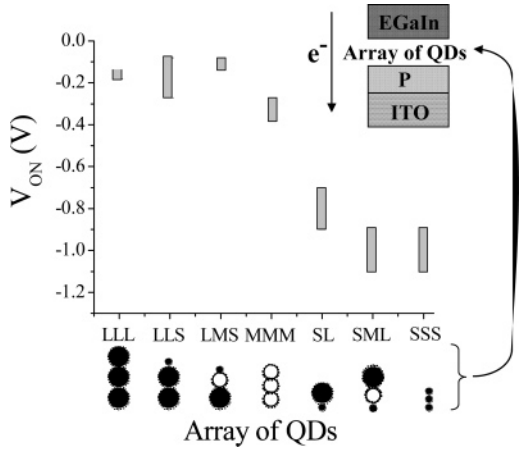

Figure 7. Ranges for the turn-on voltage (V_{ON}) for all of the junctions studied (Table 1). The Supporting Information explains the procedure used to estimate V_{ON}. The diagram in the upper right corner of the plot shows the orientation of the arrays of QDs (listed with schematics along the *x*-axis) in the junction.

Table 1. Turn-On Voltage (V_{ON}), Change in Free Energy (ΔG), and Activation Barrier (E_A) for the Reaction $QD^-/(PEDOT:PSS)^+ \rightarrow QD/PEDOT:PSS$) for the Junctions ITO/P/**X**/EGaIn

X	V_{ON} (V)[a]	ΔG (eV)	E_A (eV)[b]
LLL	−0.13 → −0.18	−0.58	0.58
MMM	−0.28 → −0.38	−0.69	0.87
SSS	−0.90 → −1.1	−0.78	1.2
LLS	−0.08 → −0.28	−0.58	0.58
LMS	−0.08 → −0.13	−0.58	0.58
SL	−0.70 → −0.90	−0.78	1.2
SML	−0.90 → −1.1	−0.78	1.2

[a] The turn-on voltage is given as a range ($V_1 \rightarrow V_2$); see the text for the procedure for estimating the range. [b] See eq 2b; for this calculation, λ = 0.1 eV.

heat)—at the interface resulted in net flow of electrons from the EGaIn to the ITO.[64]

What Determines V_{ON}? For each junction, we observed a turn-on voltage, V_{ON}—that is, a value of V at which "significant" current (current beyond that caused by leakage of thermally excited or photoexcited electrons to or from the external circuit) began to flow through the device. The Supporting Information contains the specific procedure we used to estimate V_{ON} from the plots of $\langle J \rangle_{log}$ vs V for each array. We also estimated V_{ON} from the plots of the lower and upper error bars of $\langle J \rangle_{log}$ vs V (Figure 5c); these three values of V_{ON} defined the range in Table 1 and Figure 7.

(1) Identification of the Current-Limiting Step in the Flow of Electrons from EGaIn to ITO. It is clear that $|V_{ON}|$ was lowest for the junctions where the *large* QDs were adjacent to the PEDOT:PSS and highest for the junctions where the *small* QDs were adjacent to the PEDOT:PSS. This order suggests that the step that determines the magnitude of the current through the device is step (iii) (from the list above): the electron transfer from the reduced QD (the QD having an extra electron) to the electron-deficient PEDOT:PSS—that is, the annihilation reaction $(PEDOT:PSS)^+/QD^- \rightarrow$ PEDOT:PSS/QD. It appears that the larger the gap between the energy of the LUMOs of the QDs at the interface and the energy of the VB of PEDOT:PSS (Figure 6), the larger the applied electric field needed to induce this reaction.

(2) What Dictates the Rate of the Charge Annihilation Reaction at the Interface between the QDs and PEDOT:PSS? Marcus Theoretical Analysis. The importance of energetic alignment of states of the electron donor and states of the acceptor (here, the electron donor is the reduced QD (QD^-) and the electron acceptor is the oxidized polymer, $(PEDOT:PSS)^+$) for conduction of electrons across an interface between an active material and its electrode is well-recognized.[65,66] It is nonetheless useful to outline in detail why the annihilation reaction $(PEDOT:PSS)^+/QD^- \rightarrow$ PEDOT:PSS/QD, which is exothermic ($\Delta G < 0$) for all three sizes of QDs, required an electric field to occur, and why the rate of this reaction depended inversely on the magnitude of the gap between the LUMOs of the QDs and the valence band of the PEDOT:PSS.

We can begin to answer these two questions with an expression for the rate constant, k_{ET}, for an electron-transfer reaction between two components that are not intimately electronically coupled (through a highly conjugated series of covalent bonds) (eq 1a,b).

$$k_{ET} = \frac{2\pi}{\hbar} V_{el}^{\ 2}\, FC \tag{1a}$$

$$FC = \sum_i \sum_j \rho_i \langle \chi_{Pj} | \chi_{Ri} \rangle^2 \delta(\epsilon_{Pj} - \epsilon_{Ri}) \tag{1b}$$

These equations, which are derived from Fermi's Golden Rule,[67] give the rate of a transition from a vibronic manifold of reactant states $\{i\}$ to a vibronic manifold of product states $\{j\}$, with two assumptions: (i) that the Born−Oppenheimer approximation is valid and (ii) that the system is in thermal equilibrium—that is, the population of the states in the reactant manifold follows a Boltzmann distribution (ρ_i).[68] In eq 1a,b, χ_{Ri} and χ_{Pj} are the equilibrium nuclear wavefunctions for the reactant ($(PEDOT:PSS)^+/QD^-$) at level i (with energy ϵ_{Ri}) and product (PEDOT:PSS/QD) at level j (with energy ϵ_{Pj}), respectively, and V_{el} is the overlap of the electronic wavefunctions of the reactant and product (across the layer of organic surfactant on each QD). The delta function $\delta(\epsilon_{Pj} - \epsilon_{Ri})$ (= 1 for $\epsilon_{Pj} = \epsilon_{Ri}$ or 0 for $\epsilon_{Pj} \neq \epsilon_{Ri}$) expresses the important requirement that the transition can only occur at a nuclear configuration where the reactant and product states are degenerate in energy, such that the energy of the electron is conserved in the tunneling event.[67] The thermally averaged vibronic overlap between the potentials of the reactant and product states—that is, the set of probabilities that the reactant and product species will simultaneously be in nuclear configurations that are energetically degenerate—is the Franck−Condon weighted density of states (FC).[69,70]

Equation 1a,b implies that the greater the overlap (energetically) of the densities of states of the reactant and product—i.e., the bigger the value of FC—the faster the reaction. Marcus

(64) The oxidation potential of the QDs is too high for electrons from the HOMOs of the QDs to recombine with holes from the PEDOT:PSS (Figure 6).

(65) Tseng, Y.-C.; Phoa, K.; Carlton, D.; Bokor, J. *Nano Lett.* **2006**, *6*, 1364.
(66) Makinen, A. J.; Hill, I. G.; Kinoshita, M.; Noda, T.; Shirota, Y.; Kafafi, Z. H. *J. Appl. Phys.* **2002**, *91*, 5456.
(67) Cohen-Tannoudji, C.; Diu, B.; Laloe, F. *Quantum Mechanics*; John Wiley and Sons: New York, 1977; Vol. 2, p 1300.
(68) Bolton, J. R.; Archer, M. D. *ACS Adv. Chem. Ser.* **1991**, *228*, 7.
(69) Marcus, R. *Rev. Mod. Phys.* **1993**, *65*, 599.
(70) Gosavi, S.; Marcus, R. A. *J. Phys. Chem. B* **2000**, *104*, 2067.

developed a method by which FC is expressed as a function of ΔG and a parameter called the reorganization energy (λ).[71−73] The reorganization energy is that needed to reorganize the reactant and product (and the solvent molecules, if present; here, surfactant molecules) into geometries in which the electron transfer can take place. In addition to its traditional role in predicting rate constants in solution-phase molecular systems and proteins,[68,74] Marcus theory has proven a valuable tool to describe electron transfer between identical QDs,[10] between molecules and TiO_2 nanocrystals within dye-sensitized solar cells,[75] across metal−organic interfaces,[70,76] and between CdSe and TiO_2 QDs.[77]

In Marcus theory, the electron transfer is coupled to a single averaged nuclear mode of energy, $\hbar\omega$ (such that $\lambda = S\hbar\omega$, where S is the Huang−Rhys factor, the strength of the coupling between the electronic transition and the relevant vibration). The potential surfaces of the reactant and product thereby reduce to two parabolas whose minima are separated in potential energy by ΔG. In the classical limit (where $kT > \hbar\omega/4$), FC converges to the form in eq 2a, where the activation barrier for the electron-transfer reaction, E_A, is defined by eq 2b.[70]

$$\mathrm{FC} = \frac{1}{\sqrt{4\pi\lambda kT}} \exp(-E_A/kT) \tag{2a}$$

$$E_A = \frac{(\Delta G + \lambda)^2}{4\lambda} \tag{2b}$$

In eq 2b, the reorganization energy, λ, is always positive, and for an exothermic reaction (like we are considering), ΔG is negative.

Here, we assume that the charge annihilation reaction $(PEDOT:PSS)^+/QD^- \rightarrow$ PEDOT:PSS/QD is coupled only to the C=C stretching mode within the PEDOT chains ($\hbar\omega \approx 1500$ cm^{-1}).[73,78] Since $kT > \hbar\omega/4$, we can use the classical Marcus equations (eq 2a,b) to calculate the barriers for this reaction. Estimating λ in doped conducting polymers is complicated, due to the effects of counterion stabilization and the "pre-reorganization" of nuclei upon doping. A reasonable estimate for λ is 0.1 eV ($S = 0.54$), which is approximately the internal reorganization energy for the process of positively charging and discharging pentacene, which, like doped PEDOT, is a flat, highly conjugated organic system.[73,79]

Table 1 contains the values of ΔG (in eq 2b) for the reaction $(PEDOT:PSS)^+/QD^- \rightarrow$ PEDOT:PSS/QD for each of the junctions. We approximate ΔG as the difference in energy between the VB of PEDOT:PSS and the LUMO of the QDs in the adjacent layer (the next section discusses the additional contribution of Coulomb forces to the free energy difference between these two states). For all of the junctions, $\Delta G > \lambda$; this reaction is therefore in the so-called Marcus inverted region.[70] In the inverted region, as ΔG increases, E_A increases (eq 2b). Qualitatively, the activation barrier E_A is caused by a decrease in the vibronic overlap (or Franck−Condon factor, FC) between reactant and product surfaces as their minima are moved farther apart energetically. Table 1 contains the values of E_A for this reaction for each of the junctions, calculated using eq 2b. As the QDs at the interface with PEDOT:PSS get smaller in size, the energetic barrier for charge transfer increases (E_A = 0.58 eV (L**X**), 0.87 eV (M**X**), 1.2 eV(S**X**)), and the annihilation reaction slows. The values for E_A depend, of course, on our choice of λ, but since λ is assumed to be the same for all of the junctions, this choice does not affect our qualitative prediction for the trend in the height of the tunneling barrier as a function of the size of the QDs at the interface.

(3) Mechanism of Turn-On: A Coulomb Force Lowers the Barrier for Charge Annihilation. Before connecting our predicted trend in E_A (E_A(L**X**) < E_A(M**X**) < E_A(S**X**)) to our observed trend in V_{ON} ($|V_{ON}|$(L**X**) < $|V_{ON}|$(M**X**) < $|V_{ON}|$(S**X**)), we must discuss how an increase in V might lower the tunneling barrier for the annihilation reaction. We believe that, at $|V| < |V_{ON}|$, as electrons accumulate in the QDs and holes accumulate in the PEDOT:PSS, the potential energy of electrons in the QDs near the interface decreases because they are stabilized Coulombically by the presence of positive charges in the adjacent PEDOT:PSS. The resultant Coulomb force on the electrons and holes lowers the barrier for electrons to travel across the interface caused by the offset in energy levels. The height of the barrier therefore determines the magnitude of the force—and, in turn, the magnitude of V—that is necessary to precipitate annihilation. On the basis of our calculations of E_A using Marcus theory, we would then predict that $|V_{ON}|$(L**X**) < $|V_{ON}|$(M**X**) < $|V_{ON}|$(S**X**); this order is the one we observed (Figure 7 and Table 1).[80]

We note that neither a "band-bending" picture[36] nor the Marcus picture can readily explain the eventual turn-on of the junction as a result of this accumulation of charge: The band-bending picture describes a process in which the energies of electrons that accumulate in the layer of QDs near the interface with PEDOT:PSS increase (and the energies of electrons in the PEDOT:PSS near the interface decrease) as $|V|$ increases due to increased (or decreased) electron−electron repulsion in these regions. This process brings the electron-donating and electron-accepting states in the two materials *farther* out of energetic resonance and therefore *hinders* charge annihilation. Marcus theory predicts that the probability for the reaction would stay fairly constant as $|V|$ increases, because accumulation of electrons and holes at the interface would destabilize both the reactant ($(PEDOT:PSS)^+/QD^-$) and the product (PEDOT:PSS/QD) states (which are interchangeable by the movement of only one electron) approximately equally, in which case ΔG (and, therefore, E_A) would be constant with increasing V.

(71) Marcus, R. A. *J. Chem. Phys.* **1965**, *43*, 679.
(72) Marcus, R. A. *J. Chem. Phys.* **1984**, *81*, 4494.
(73) Olivier, Y.; Lemaur, V.; Bredas, J. L.; Cornil, J. *J. Phys. Chem. A* **2006**, *110*, 6356.
(74) Dutton, P. L.; Mosser, C. C. *Proc. Natl. Acad. Sci. U.S.A.* **1994**, *91*, 10247.
(75) Clifford, J. N.; Palomares, E.; Nazeeruddin, M. K.; Graetzel, M.; Nelson, J.; Li, X.; Long, N. J.; Durrant, J. R. *J. Am. Chem. Soc.* **2004**, *126*, 5225.
(76) Miller, R. J.; McLendon, G. L.; Nozik, A. J.; Schmickler, W.; WIllig, F. *Surface Electron-Transfer Processes*; VCH: New York, 1995.
(77) Robel, I.; Kuno, M.; Kamat, P. *J. Am. Chem. Soc.* **2007**, *129*, 4136.
(78) It is possible that there is some coupling of the charge annihilation reaction to vibrational modes in the QDs—probably the long optical (LO) phonon ($h\omega$ = 210 cm^{-1}), the out-of-phase vibration of Cd and Se atoms—but, even if $S = 1$, this coupling (0.026 eV) is much smaller than that estimated for coupling to vibrations in the polymer [Nirmal, M.; Brus, L. E. *Acc. Chem. Res.* **1999**, *32*, 407].
(79) Gruhn, N. E.; da Silva Filho, D. A.; Bill, T. G.; Malagoli, M.; Coropceanu, V.; Kahn, A.; Bredas, J. L. *J. Am. Chem. Soc.* **2002**, *124*, 7918.

(80) Figure 7 shows that $|V_{ON}|$(SSS) ~ $|V_{ON}|$(SML) > $|V_{ON}|$(SL). We believe that, for a given $|V| < |V_{ON}|$, the greater the resistivity of the array, the fewer electrons present at the interface between the QDs and PEDOT:PSS, and the smaller the Coulomb force that is available to precipitate annihilation of charge. Figure S4 shows that the junction SL is less resistive than SML and SSS.

Conclusions

Summary. This paper compares the current density−voltage ($J-V$) response for junctions containing an array of a single size of CdSe QDs to that of junctions containing an array of multiple sizes of QDs (Figure 1). This new approach for analyzing the electrical characteristics of junctions containing QDs enabled us to partition the $J-V$ response of the junctions into size-dependent effects at the interfaces between the QDs and the electrodes and size-dependent effects within the array.

The plots of J vs V for the ITO/PEDOT:PSS/QD/EGaIn junctions (Figure 5) were asymmetric in the range of V that we examined: electrons did not flow from ITO to EGaIn, primarily because we did not supply enough energy for electrons in the PEDOT:PSS to enter the LUMOs of the QDs, or for electrons in the HOMOs of the QDs to enter the EGaIn (Figure 6). Electrons did flow in the opposite direction (from EGaIn to ITO), after application of a threshold voltage, V_{ON}, the value of which depended primarily on the size of the QDs next to the PEDOT:PSS (Figure 7). This observation leads us to conclude that the current-limiting step in transport of electrons from EGaIn to ITO was the annihilation of electrons and holes at the interface between the QDs and PEDOT:PSS, i.e., the reaction $QD^-/(PEDOT:PSS)^+ \rightarrow QD/PEDOT:PSS$.

At $|V| < |V_{ON}|$, this reaction was slow due to a tunneling barrier caused by a gap between the energies of the electron donor (the partially filled HOMO of QD^-) and the electron acceptor (the valence band of $(PEDOT:PSS)^+$). We estimate the size of this barrier from the size of the energy gap and the parameter λ (the reorganization energy), using Marcus formalism (eq 2b). Our prediction that the height of the barrier would increase as the size of the QDs at the interface between the QDs and PEDOT:PSS decreased qualitatively explains the trend we observed: $|V_{ON}|(\mathbf{LX}) < |V_{ON}|(\mathbf{MX}) < |V_{ON}|(\mathbf{SX})$. We hypothesize that, at V_{ON}, the Coulomb force between accumulated positive charges in the PEDOT:PSS and negative charges in the QDs at the interface lowered the barrier and induced the annihilation reaction; this proposed mechanism is analogous to image-potential lowering of tunneling barriers at metal−semiconductor contacts.[36]

We believe that, at $|V| > |V_{ON}|$, charge annihilation occurs readily at the interface between the QDs and the PEDOT:PSS, so the observed current should be limited by transport of electrons through interfaces between the QDs. Initial experiments and analysis indicate that the dependence of J on V at $|V| > |V_{ON}|$ fits to a model for current limited by sequential tunneling from QD to QD, where the resistivity of the array decreases as the QDs become charged with electrons injected from the EGaIn. We are currently attempting to clarify how the size of the QDs in a given layer influences the degree to which charges accumulate in that layer, and how the overall distribution of charge affects the observed resistivity of the junction.

Implications for Devices Based on QDs: Higher Yield of Exciton Separation in Heterojunction Solar Cells. Heterojunction solar cells are composed of two different materials—one *n*-type, one *p*-type. Ideally, photoexcited electron−hole pairs (excitons) in both materials migrate to the interface at which the materials meet, and spontaneous charge transfer occurs to create negative charges in the *n*-type material and positive charges in the *p*-type material. One major source of inefficiency in these devices is recombination (due to Coulombic attraction) of newly separated holes and electrons at the interface between the two materials.

Our work suggests strategies for improving the performance of a heterojunction solar cell. Specifically, in a heterojunction between QDs and a polymer, charge recombination at the interface between the two materials is the combination of a hole in the valence band of a polymer and the electron in the LUMO of a QD; this reaction is analogous to the electron−hole annihilation reaction we studied here. By varying the size of the QD at the interface between the QDs and PEDOT:PSS, we found that the annihilation reaction slows as the gap between the partially filled LUMO of the neutral QD (i.e., HOMO of QD anion) and the valence band of the $(PEDOT:PSS)^+$ increases. If we were to replace PEDOT:PSS in the devices described here with an electron-donating polymer in a heterojunction solar cell, we would choose the smallest QD possible to place at the interface between the QDs and the polymer in order to (i) minimize the rate of the nonproductive charge recombination reaction and (ii) match, as closely as possible, the energy of the LUMO of the QD with that of the LUMO of the polymer ($E_{LUMO} \approx -3.1$ eV for poly[2-methoxy-5-(2′-ethylhexyloxy)-1,4-phenylene-vinylene] (MEH-PPV),[81] and $E_{LUMO} \approx -3.5$ eV for poly(3-hexylthiophene) (P3HT),[82] for example), in order to increase the rate of the charge separation reaction (assuming this reaction is also in the Marcus inverted region).

Acknowledgment. We acknowledge funding from NSF CHE-0518055 (Harvard), the NSEC Program of the National Science Foundation, award no. PHY-0117795 (MIT), and the U.S. Army through the Institute for Soldier Nanotechnologies, under contract no. DAAD-19-02-0002 with the U.S. Army Research Office (MIT). The authors used the shared facilities supported by the National Science Foundation under NSEC (PHY-0117795 and PHY-0646094, Harvard), MRSEC (DMR-0213805, Harvard), and MRSEC (DMR 0213282, MIT). E.A.W. thanks the Petroleum Research Fund of the American Chemical Society for a fellowship (PRF no. 43083-AEF). V.J.P. was funded in part by the NSF MRSEC program (DMR 0213282) at MIT. The authors thank E. Lavoise for preparing the samples for TEM.

Supporting Information Available: Experimental details, procedure for determining the turn-on voltage, and Figures S1−S5, showing atomic force micrographs of the films of QDs, procedure for forming tips of EGaIn, and additional $J-V$ data. This material is available free of charge via the Internet at http://pubs.acs.org.

JA076438H

(81) Petrella, A.; Tamborra, M.; Curri, M. L.; Cosma, P.; Striccoli, M.; Cozzoli, P. D.; Agostiano, A. *J. Phys. Chem. B* **2005**, *109*, 1554.
(82) Al-Ibrahim, M.; Roth, H.-K.; Schroedner, M.; Konkin, A.; Zhokhavets, U.; Gobsch, G.; Scharff, P.; Sensfuss, S. *Org. Electron.* **2005**, *6*, 65.